Chalmers Publication Library

CHALMERS

Copyright Notice IEEE

(Article begins on next page)

Characterization of Reverberation Chambers for OTA Measurements of Wireless Devices: Physical Formulations of Channel Matrix and New Uncertainty Formula

Per-Simon Kildal, *Fellow, IEEE*, Xiaoming Chen, Charlie Orlenius, Magnus Franzén, and Christian S. Lötbäck Patané

Abstract—The paper deals with reverberation chambers for over-the-air (OTA) testing of wireless devices for use in multipath. We present a formulation of the S-parameters of a reverberation chamber in terms of the free space S-parameters of the antennas, and the channel matrix in the way this is known from propagation literature. Thereby the physical relations between the chamber and real-life multipath environments are more easily explained. Thereafter we use the formulation to determine the uncertainty by which efficiency-related quantities can be measured in reverberation chamber. The final expression shows that the uncertainty is predominantly determined by the Rician K-factor in the reverberation chamber rather than by the number of excited modes, assumed by previous literature. We introduce an average Rician K-factor that is conveniently expressed in terms of the direct coupling between the transmitting and receiving antennas (corresponding to a line-of-sight contribution) and Hill's transmission formula (corresponding to a multipath or non-line-of-sight contribution). The uncertainty is expressed in terms of this average K-factor and geometrical mode stirring parameters, showing strong reduction by platform and polarization stirring. Finally the formulations are verified by measurements, and the new understanding of uncertainty is used to upgrade an existing reverberation chamber to better uncertainty.

Index Terms—Antenna measurements, Rayleigh fading, reverberation chamber, Rician K-factor.

I. INTRODUCTION

THE reverberation chamber is a shielded room having metallic, electromagnetically reflective walls. When a radiating antenna is located inside the chamber, it will excite some of the cavity modes that have resonances near the frequency of radiation [1], [2]. These modes interfere locally with each other and result in a statistical spatial distribution of maximum and minimum field amplitudes (i.e., hot and cold

spots) throughout the chamber. When a receiving antenna is located inside this environment, the induced voltage at its port takes on an arbitrary value as well. However, the maxima and minima of the induced voltage will generally not coincide with the maxima and minima of a specific field component in the chamber (unless the antenna is a linearly polarized probe). The maxima and minima will depend on the location and orientation of the antennas inside the chamber, and also on their polarizations and far field radiation functions [3]. The induced voltage at the antenna port will change when mechanical objects inside the chamber are moving, in continuous or stepwise manner – referred to as mechanical mode stirring. Then, the induced voltage will experience similar statistical maxima and minima variations as when the antenna moves to different positions and orientations, i.e., fading. This variation of the induced voltage makes it possible to use reverberation chambers for testing of antennas and wireless devices subject to fading. Such testing in realistic fading environments is now commonly referred to as OTA (over-the-air) testing, in contrast to the conductive tests that were done previously, i.e., by connecting cables directly between the test instrument and the receiver input on the wireless terminal. The purpose of the present paper is to describe and characterize the reverberation chamber as a statistical fading emulator for testing of antennas and wireless devices, and in particular when the antennas and devices make use of antenna diversity and MIMO (multiple input multiple output) multiport technology.

For an electrically large reverberation chamber there will be many excited modes at the frequency of operation. For such case, during mechanical mode stirring, it was theoretically claimed and experimentally verified in [4] that the real and imaginary parts of the rectangular components of the electric and magnetic fields throughout the chamber are independently Gaussian distributed, with identical variances. This is also the result of interference of the spectrum of the large number of independent plane waves present in the reverberation chamber [3]. These plane waves can readily also be expressed from an expansion of the excited cavity modes inside the chamber; there are actually eight plane waves per mode excited [5]. The induced voltages at the port of a receiving antenna located inside the reverberation chamber will be a linear combination of such plane waves weighted by the far field function of the antenna, and therefore the real and imaginary parts of the induced

voltages at the ports of the receiving antenna will be Gaussian distributed as well, i.e., complex Gaussian distribution of the complex induced voltage. The complex Gaussian distribution can be regarded as a result of the central limit theory [4], provided there are enough excited modes and plane waves with arbitrary independent amplitudes, polarizations and phases. This complex Gaussian distribution is in turn known to result in a Rayleigh distributed absolute value of the induced voltage, i.e., Rayleigh fading, and the received power is correspondingly exponentially distributed, all according to classical theory of statistics. However, it has been observed in many practical measurement setups that there also exists an unstirred constant field component, that is not affected by the mode stirring [6], and this has been used to propose the generation of a controlled Rician fading distribution [7] for advanced testing capability. The present paper will provide a complete and compact description of the complex wireless channel through the chamber, including both the stirred complex Gaussian component and the unstirred component, in terms of the free space S-parameters of the transmit and receive antennas and the chamber geometry.

The reverberation chamber was traditionally used for EMC testing of radiated emissions and susceptibility [8]. However, we can use the reverberation chamber to emulate a fading environment for repeatable tests of electronic devices with small antennas, such as cell phones and other wireless terminals for use in such fading environments, as first demonstrated in [9] and overviewed in general terms in [10]. The reverberation chamber represents (to first order and if it is large enough) a so-called rich isotropic multipath environment where the angles of arrivals (AoA) of the excited plane waves are distributed uniformly over the whole surrounding unit sphere [3], [5]. This makes the chamber particularly well suited for test purposes because classical efficiency-related quantities such as antenna radiation efficiency and total radiated power of active devices can be measured with good accuracy, and in addition we can achieve repeatable measurements of diversity gain and maximum available capacity of multiport antenna systems with MIMO capability [11]–[13], as well as receiver sensitivities in terms of bit error rates (BER) and related quantities of wireless terminals during reception [14]–[16], and throughput data rate of complete wireless systems [17].

The anechoic chamber is the traditional "free-space-type" reference environment for measuring directive gain and sidelobes of antennas designed for line-of-sight (LOS) systems, whereas the reverberation chamber has become a rich isotropic multipath reference environment for characterizing antennas for use in environments with fading [18]. The purpose of the present paper is to derive simple new S-parameter-based formulas for the reverberation chamber to provide a better explanation than formulations given before of its fundamental characteristics for testing of wireless devices including measurement uncertainty. The formulation includes the average mode bandwidth that is equal to the coherence bandwidth of the channel (if properly defined), and the inverse of the time delay spread [19]. These quantities were also measured in [20].

The first expression for the measurement uncertainty of the reverberation chamber for testing of efficiency-related quantities was published in [4], stating that the standard deviation is inversely proportional to the square root of the number of independent samples in the chamber. This should improve with frequency, because the mode density and plane wave density increase with frequency squared, see e.g., [21], but this dependence is not observed in practice. Therefore, the present paper introduces a new uncertainty theory for reverberation chambers, where the main source of error is the unstirred component of the induced voltage, i.e., a direct coupling between the transmitting and receiving antenna not affected by the mode stirring. The formulation also includes how to reduce this unstirred component; by using a rotating platform (platform stirring) or several chamber antennas (polarization stirring). These stirring methods were introduced already in [9] and [22], respectively, to improve uncertainty in small reverberation chambers, and in the present paper we are able to properly explain in which way they actually work. The new uncertainty theory was already summarily presented in [23], whereas the present paper also provides an example where the new theory can explain how it was possible to improve the uncertainty of a given small reverberation chamber.

The reverberation chamber has also other applications than those described above, such as e.g., material characterization [24].

The paper will first describe the new S-parameter formulation of the chamber, and describe its relation to measurements in real-life environments. This formulation includes Hill's impressive power transmission formula [25] for reverberation chambers, as well as the traditional Friis' transmission formula for free space. Hill's transmission formula is also modified to provide a description of the complex chamber reflection coefficient at the ports of the antennas of the chamber, which has not been published before. Thereafter, the new uncertainty model is derived, and it is applied to improve an existing reverberation chamber.

II. Description of a Typical Reverberation Chamber for OTA Testing of Wireless Devices

The present theoretical models have mainly been developed to fit the reverberation chambers shown in Fig. 1. These are the Bluetest HP reverberation chamber and the improved Bluetest Reverberation Test System RTS60, both having a size of 1.8 m × 1.7 m × 1.2 m. The chamber has a shielding isolation of 100 dB to be able to perform receiver sensitivity measurements without disturbances from exterior wireless devices like mobile phones.

The modes excited inside this chamber can to the first order be approximated by the modes of the clean ideal rectangular cavity itself. Then, the modes combine in such a way that the boundary conditions of the total fields become zero at additional metal objects inside the chamber (such as the two mechanical plate-shaped mode stirrers), and are otherwise satisfied at objects of other types of materials, such as a head phantom, the antennas and the device under test (DUT). The satisfaction of the boundary conditions may not be possible with the original modes, so that new perturbed modes are formed in the actual non-ideal rectangular cavity with all stirrers and objects present. These modes have slightly different resonance frequencies than the original clean ideal cavity modes. When the mechanical stirrers move, the resonance frequencies of these new modes may
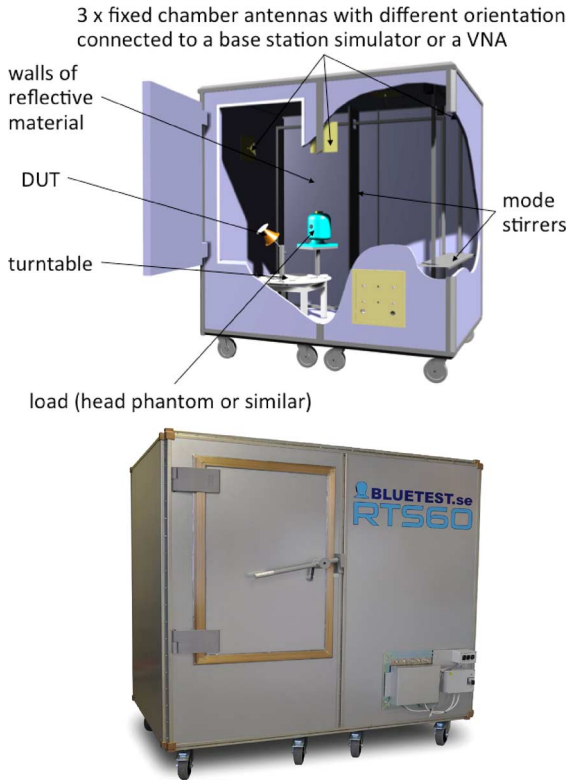
Fig. 1. Drawing (upper) of Bluetest HP reverberation chamber, and photo (lower) of the improved Bluetest RTS60 system (www.bluetest.se).

change, and they recombine in different ways, thereby creating the complex Gaussian field distribution.

The most common mechanical mode stirrer is an arbitrarily shaped metallic rotating paddle. Such rotating paddle is designed to be nonsymmetrical, and can stir at a continuous rate or in stepwise manner, referred to as continuous and stepped mode stirring, respectively. In the latter case the paddle stops at predetermined positions for each measurement. In the Bluetest chambers the mechanical mode stirrers has the form of two metal plates that are moved along two orthogonal walls. Both plates are flat and with rectangular shape, except for the fact that the outer 20 mm on each side of their cross section is bend 90 degrees with respect to the rest of the surface of the plate to provide stiffness. For the HP chamber one plate is 30 cm $\times$ 160 cm and is located vertically and moved 140 cm horizontally along the back wall, and the other is 88 cm $\times$ 30 cm in size and is located horizontally and moved 145 cm vertically along the right wall, both as shown in the drawing in Fig. 1. In the RTS chamber the second plate is the same whereas the first one is replaced by a 97 cm $\times$ 40 cm sized plate that is located horizontally along the roof and moved 125 cm along the roof. Thereby, the plates cover two large and "orthogonal" volumes, each of them almost equal to the area of the associated wall multiplied with the width of the plates, without occupying any space in the central part of the chamber where the DUT is located. Both these plates can be moved continuously (often referred to as fast mode), or stepwise. The plates can be run in different sequences relative to each other, but in the present paper they only run simultaneously and step-wisely from one end to the other, except for the additional measurements with continuous movements in the two last graphs in Fig. 9.

Another method of mode stirring relies on varying the position and/or orientation of either the transmitting or receiving antenna inside the chamber, or both. This can be achieved by placing one of the antennas on a controlled platform such as a turntable (either in continuous or stepped mode) or by manually changing the position and orientation of the antenna between each measurement. This is called *platform,*[9] and *position stirring,* respectively. These methods will also change the field boundary conditions inside the chamber in the same way as the mechanical plate stirrers do, although the main effect of these stirring methods is the change of positions and orientations of the antenna so that it receives the given waves in the chamber with different phases and amplitudes via a movement and rotation of its far field function. Thereby, the waves recombine in completely different ways when the position and orientation of the antenna is changed, and create the complex Gaussian distribution of the received voltage. A variant of position stirring was used in the theoretical study in [26] based on using the computer code in [27], where the Green's function of the cavity is described in terms of clean ideal cavity modes. The position stirring was then done by moving the transmitting and receiving small antennas around in different positions in the whole chamber volume, except too close to the walls and to each other.

A third method of perturbing the modes is by means of a *multi-probe system*, i.e., by means of an array of antennas positioned across the chamber, preferably wall-mounted to save space. In such setup, each antenna is employed one after the other, resulting in as many different independent samples of the transfer function as there are antennas. This method speeds up measurement time if electronic switching between the antennas is employed. It complicates that every antenna has its own mismatch factor for which the average power transfer function has to be compensated. The multi-probe system consists in the Bluetest HP chamber of three orthogonal wall-located chamber antennas and is referred to as polarization stirring [22], because it can be used to obtain polarization balance in the chamber, i.e., so that the average power transfer function of a simple dipole antenna become the same independently of how it is oriented. In the Bluetest RTS chambers the three chamber antennas are located on three orthogonal walls of a cube located behind a 99 cm tall and 2×50 cm wide metal shield shaped like a metal corner standing on the floor of the chamber.

These different stirring methods are in the Bluetest chambers combined to improve uncertainty.

The Bluetest chamber can also be loaded with absorbing objects to control the average mode bandwidth (defined in Section III) and thereby the coherence bandwidth and time delay spread in the chamber, as shown in Table I and described in [19]. The coherence bandwidth is equal to the average mode bandwidth in the chamber, when the former is defined as the half-bandwidth at which the complex correlation function has a value of $B_c = 0.5$, and the time delay spread is given by (27). For more details and description of the loads, see [19].

III. THEORY OF S-PARAMETERS MEASURED IN REVERBERATION CHAMBER

The measurement setup for calibration and passive efficiency and MIMO antenna measurements is shown in Fig. 2. This

TABLE I
APPROXIMATE COHERENCE BANDWIDTHS AND TIME DELAY SPREADS FOR
DIFFERENT LOADINGS OF THE REVERBERATION CHAMBER IN FIG. 1 OVER THE
FREQUENCY RANGE 1.2 – 2.7 GHz

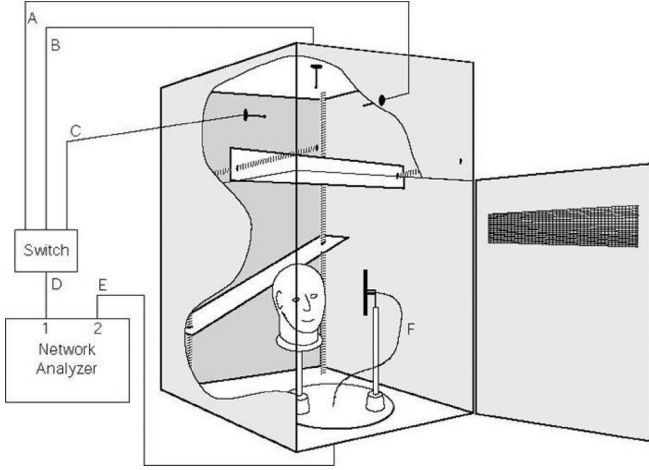| Load	Average mode bandwidth = Coherence bandwidth	Time delay spread
Empty	2 - 1 MHz	150 - 220 ns
Head phantom	3 - 3 MHz	100 - 130 ns
+3 extra cylinders with absorbers	7 MHz	40 ns
+ 6 extra cylinders with absorbers	10 MHz	30-25 ns

Fig. 2. Illustration of reverberation chamber with measurement setup for calibration and measurement of MIMO antenna. This reverberation chamber is provided with two mechanical plate stirrers, platform stirring and polarization stirring. The latter are three wall-mounted chamber antennas, and one calibration/reference antenna located at the rotate-able platform.

gives the S-parameters between ports 1 and 2 of the vector network analyzer (VNA). We will in the following assume that the measurement setup is calibrated in such a way that the complex S-parameters are referred to the actual ports of the three chamber antennas A, B and C used for polarization (multi-probe) stirring, and the reference antenna F. We will for simplicity here only give the S-parameters between two antennas in the chamber, but the equations are readily extended to multi-port case by standard approaches.

We can physically argue that S_{11} of an antenna in the chamber must consist of two contributions; one contribution being the S_{11}^a from the antenna itself as if it was located in free space, and another "channel-type" contribution H_{11}^c from the chamber (see Fig. 3), i.e.,

$$S_{11} = S_{11}^a + H_{11}^c. \tag{1}$$

The former S_{11}^a contribution is deterministic and can be referred to as the LOS contribution, although it may also be effected by a wall of the chamber if the antenna is located at or close to this wall or pointing towards it, or even by several walls if the antenna is pointing into a corner between two or three walls. Therefore, we may need to interpret the "free space" as all the "other" walls being removed except the closer one(s).
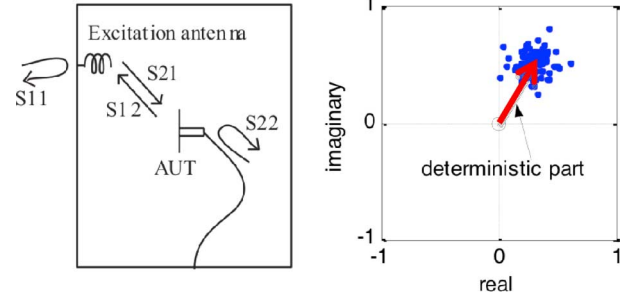

Fig. 3. Definition of S-parameters of two antennas in a reverberation chamber (left), and illustration of deterministic and random contributions to them (right). The random contribution is a result of the mode stirring.

The latter H_{11}^c is a random wireless channel contribution resulting from the mode stirring and can be considered to be the same as the non-line-of-sight (NLOS) multipath contributions in real-life environments. If the number of independent values of H_{11}^c is large enough, it will have a complex Gaussian distribution with zero mean as explained in the introduction. Therefore, it is possible to determine S_{11}^a by complex averaging of the measured S_{11} over all M stirrer positions, as shown in [28], i.e.,

$$S_{11}^a = \frac{1}{M} \sum_M S_{11} = \overline{S_{11}} \tag{2}$$

where $\overline{S}_{11}$ is a compact way of writing the average of S_{11}. We will use this notation throughout the paper. Similarly, we can find S_{22}^a of the other antenna connected to port 2 of the VNA.

We can argue in the same way that S_{21}, i.e., the voltage at port 2 resulting from a source at port 1, must consist of two combined wireless channel contributions (Fig. 3), one deterministic H_{21}^d being the same as in free space, and another statistic contribution H_{21}^c coming from the chamber, i.e.,

$$S_{21} = H_{21}^d + H_{21}^c. \tag{3}$$

The deterministic part can be estimated by complex averaging of S_{21} over all stirring positions M, in the same way as for S_{11}, by the formula

$$H_{21}^d = \frac{1}{M} \sum_M S_{21} = \overline{S_{21}}. \tag{4}$$

This is not possible when polarization (i.e., multi-probe), position or platform stirring is employed, because in these cases the "free space" direct coupling will vary during stirring. However, we will later in Section V.C introduce an average Rician K-factor that can be used to deal with this.

We will in (5), (6) and (8) give expressions for H_{21}^d and the expected power averages of the statistical channels H_{11}^c and H_{21}^c, respectively.

A. Friis' Transmission Formula for the Deterministic Direct Coupling = LOS Contribution

We would like the reverberation chamber to provide an isotropic environment, in order to make the measured results independent of orientation of the reference antenna and DUT. Therefore, we would like the direct coupling in (3) to be as low as possible. The direct coupling follows the well-known

classical free-space transmission formula, also known as Friis' transmission formula, i.e.,

$$G_{direct} = \left|H_{21}^d\right|^2 = \left(\frac{\lambda}{4\pi r}\right)^2 G_t G_r \qquad (5)$$

where r is the distance from the chamber antenna to the reference antenna (or the DUT) inside the chamber, λ is the wavelength, and G_t and G_r are the realized gains of the chamber antenna and reference antenna (or DUT), respectively, in the direction of each other. To minimize this contribution, the main lobes of the antennas *should not* point towards each other. Polarization stirring and platform stirring are also very effective in reducing direct coupling, because the direction of the chamber antenna or the DUT, respectively, will be different for each stirrer position, thereby removing the effect of H_{21}^d by "stirring" it. (Note that in average $\left|H_{21}^d\right|^2$ is also proportional to efficiency. Therefore, the LOS contribution can also be used to measure efficiency related quantities, provided we have enough platform positions and chamber antennas, so that the directions of incidence on the AUT/DUT covers the whole unit sphere. The extreme case is an anechoic chamber for which we only have direct coupling, and efficiency can be measured by averaging over all directions in space). Direct coupling, together with loading of the chamber, can be used to obtain a controlled Rician distribution for test purposes, as proposed in [7].

From the discussion in the previous subsection, it is clear that the reverberation chamber provides Rayleigh fading if the direct coupling is reduced to the point that it is *negligible compared to* the chamber's random contribution to S_{21}. This reduction can be achieved by platform stirring, or by using chamber antennas that display a null in the direction of the AUT/DUT. In [5] it was shown that each mode in a rectangular cavity can be expressed as eight plane waves, and that the directions of arrival of these plane waves are uniformly distributed over the unit sphere if there are enough modes excited. Therefore, the reverberation chamber represents an isotropic multipath environment, provided the LOS component is small enough. The rich isotropic environment enables accurate measurements of quantities like radiated power and efficiency [10].

B. Hill's Transmission Formula for the Statistic Chamber Contribution = NLOS Contribution

The transmission between two antennas in free space follows Friis' transmission formula (5). The corresponding formula for transmission between two antennas located in a reverberation chamber is described by Hill's transmission formula, which is derived in [25]. The derivation is based on physical arguments and power conservation, and the formula is valid when there is negligible direct coupling and the chamber is large with many excited modes. We refer to Hill's formula as the average power transfer function, and we will use it in the following form:

$$G_{chamber} = \overline{\left|H_{21}^c\right|^2} = \frac{P_r}{P_t} = \frac{c^3 e_{totrad1} e_{totrad2}}{16\pi^2 V f^2 \Delta f} \qquad (6)$$

where $\overline{\left|H_{21}^c\right|^2}$ is a compact way of writing the average of $\left|H_{21}^c\right|^2$ over all stirrer positions, f is the frequency, c is velocity of light, V is the chamber volume, $e_{totrad1}$ and $e_{totrad2}$ are the total

radiation efficiencies including mismatch of the two antennas, and Δf is the average mode bandwidth. The latter consists of four additive contributions due to wall losses, leakage, antennas in the chamber, and absorbing objects, i.e.,

$$\Delta f = \sum_{\substack{all \\ walls}} \Delta f_{wall} + \sum_{\substack{all \\ slots}} f_{slot}$$
$$+ \sum_{\substack{all \\ antennas}} \Delta f_{antenna} + \sum_{\substack{all\ lossy \\ objects}} \Delta f_{object} \qquad (7)$$

according to [25] by substituting $\Delta f = f/Q$, with

$$\Delta f_{wall} = \frac{2A}{3V}\sqrt{\frac{c\rho f}{\pi\eta}}, \qquad \Delta f_{slot} = \frac{c\sigma_l}{4\pi V},$$
$$\Delta f_{antenna} = \frac{c^3 e_{totrad}}{16\pi^2 V f^2}, \qquad \Delta f_{object} = \frac{c}{2\pi V}\sigma_a$$

and where V is the chamber volume, η the free space wave impedance, A the area of a conducting surface (such as a chamber wall) with surface resistance ρ, σ_l is the leakage cross section of a narrow slot in the chamber wall, and σ_a is the average absorption cross section of an absorbing object. Hill describes in [25] how to calculate σ_l and σ_a; both having slow frequency variation compared to the explicit frequency variation in the formulas. Hill's formula for the effect of the absorption cross section σ_a has in [29] been validated by numerically computing it for a lossy cylinder and measuring it in a reverberation chamber.

The expected average power of the wireless channel reflection contribution H_{11}^c in (1) is given by the same Hill's formula (6), except that the average power is a factor of 2 larger, i.e.,

$$\overline{\left|H_{11}^c\right|^2} = \frac{2c^3 e_{totrad1} e_{totrad2}}{16\pi^2 V f^2 \Delta f}. \qquad (8)$$

The reason for the factor two can be explained as follows: If a mode is **strongly excited** because the transmitting antenna 1 is in an interference maximum of the mode, it will also be **received strongly** because the receiving antenna 1 is the same. Thus, there is a correlation between the transmitting and receiving functions, and this will in average give a factor two larger received power than if the transmitting and receiving antennas are separate and uncorrelated, according to [30]. In practice the observed factor is smaller than two. We believe this is caused by the inaccuracies in extracting H_{11}^c from S_{11}, which is more difficult than extracting H_{21}^d from S_{21} because the deterministic part is much larger in the former. Also, one antenna excites fewer modes than two antennas, and thereby H_{11}^c contains a smaller number of independent samples than H_{21}^c.

The measurement procedures for reverberation chambers make use of the fact that the average power transfer function is proportional to the total radiation efficiency of the AUT or antenna on the DUT as shown in (6). However, this is seen only to be true if the average mode bandwidth contribution $\Delta f_{antenna}$ due to the antennas is small compared to the total Δf. Also, it is very important that the complete average mode bandwidth Δf in the reverberation chamber is the same during calibration and test. The Δf_{object} may be affected by the DUT itself, in particular if the DUT is large and contains

lossy materials. Therefore, the best way to ensure the same Δf is to have the AUT/DUT present inside the reverberation chamber during calibration with the reference antenna, and to have the match-terminated reference antenna present inside the reverberation chamber when making measurements on the AUT/DUT. However, this requires a separate calibration for each AUT/DUT so it is quite time-consuming. In practice, such extensive calibration is only needed when testing physically large mobile stations [31].

C. Average Mode Bandwidth Δf and Chamber Q

We see from (7) that when lossy objects are placed in the reverberation chamber, the average mode bandwidth is dominated by Δf_{object} that has no explicit frequency variation. It should be noted that we here in (6) and (8) have expressed the average transmission or transfer function in terms of the average mode bandwidth rather than the typical Q of the modes, which Hill used in [25]. Note that Q and Δf are related by $Q = f/\Delta f$. The reason we did this is that the formula for Δf in (7) is much more compact than the corresponding formula for Q, because the different Δf contributions are additive, while Q contributions are not. Also, for specific chambers (at least loaded ones), the average mode bandwidth will not vary much with frequency, and therefore the value of Δf characterizes the chamber better than Q over a large frequency band.

Different practical chambers can have very different values of total Δf, corresponding to a chamber Q of between 30 and several thousand. For active receiver measurements, the average mode bandwidth can be controlled to give a certain effect on the performance of the receiver due to the time delay spread and coherence bandwidth, see the relation between these quantities and Δf summarized in Table I. This is important when measuring active wireless devices, in order to control whether the fading is frequency-flat or frequency-selective, which is determined by the coherence bandwidth being larger than or smaller than the signal bandwidth, respectively, see [17]. To achieve a purely noise-limited measurement condition; we must ensure frequency-flat fading. When measuring total radiated power (TRP), the actual value of the average mode bandwidth is of less importance, as long as the power sampling instrument can handle and accurately follow the time spread signal in a high-Q cavity. Empirically, it has been shown that the most commonly used base station simulators exhibit this feature, which enables TRP measurement for a wide range of mode bandwidths. For practical reasons, a very narrow average mode bandwidth (high Q) should be avoided to keep the connection between the base station simulator and the DUT stable throughout the measurement sequence. Some mobile terminals have a tendency to turn themselves off if they experience a very rough environment with a large instantaneous mismatch S_{11} at the antenna port.

D. About Practical Measurements and Validity of Hill's Formula

In practice, measurement of radiation efficiency is based on first determining the average power transfer function of the chamber by calibration. Such a calibration is performed by using a reference antenna of known radiation efficiency e_{rad2},

with the AUT present in the chamber and terminated with a load matched to the system impedance. Thereafter, the reference antenna is match-terminated in the same way, and the AUT is connected to the VNA to perform the actual measurement. The ratio between the average transfer functions of the chamber for the two cases will be equal to the ratio between the radiation efficiencies of the reference antenna and the AUT. The radiation efficiency e_{rad1} of the chamber-antenna does not need to be known, because it will be the same both when measuring the reference antenna and the AUT. The procedure when measuring TRP and receiver sensitivity of active terminals (DUTs) is equivalent, with AUT above replaced by DUT.

Hill's formula is valid as long as many modes are excited and the direct coupling is negligible. Also, we must ensure that the performance of the AUT or the DUT is not affected by its closeness to i) the walls of the chamber, ii) the mechanical stirrers, and iii) objects used to load the chamber. It is clear that the conditions depend very much on the directivity of the AUT and the antenna on the DUT. However, antennas on wireless devices are normally small antennas with low directivity (typically smaller than 3 dB), and then it suffices to require a minimum distance of half wavelength from any wall (including floor and ceiling) or stirrer or other object inside the chamber. This is also a commonly used guideline for EMC measurements. This rule does of course not apply to objects that during measurements are to be regarded as part of the DUT, such as e.g., when the performance of a cell phone is to be evaluated in talk position relative to a head phantom.

IV. Relation to Channel Matrices of Real-Life Environments

Hill's transmission formula for reverberation chambers is very fundamental, and it has of course relevance for performance in real-life multipath environments. The most important is that the performance is determined by the total radiation efficiencies of the antennas, and not their realized gains. This fact is now quite accepted, although there has not been many studies to determine under which conditions this is true, i.e., under which conditions we can regard the rich isotropic multipath environment as being representative of real-life environments. It is clear that the statistics of the user helps making real-life environments resemble rich isotropic environments, [18] and [32], but more studies are needed to develop guidelines for how to use the test-results for evaluating performance in real-life scenarios. The rich isotropic environment is not identical to any real-life multipath environment, in the same way as the free space environment produced by anechoic chamber is not identical to any real-life environment with LOS for directive antennas. Therefore, guidelines are needed for how to use the test results. Such guidelines for using test results in anechoic chambers have already been developed, such as e.g., how high above ground a radio link antenna must be mounted in order to avoid interference from ground reflections. Similarly, we will for wireless devices in multipath need to know guidelines of how to mount antennas on e.g., laptops in order to avoid problems if they are used outdoor in non-isotropic multipath environments. Laptops are special, because they do not change orientation relative to the vertical axis, which mobile phones

will do due to user statistics, when used on both sides of the head.

V. NEW UNCERTAINTY MODEL WITH RICIAN K-FACTOR

The above S-parameter description is used to develop a new uncertainty model of reverberation chambers. The basic assumption is that we have two random processes contributing to the average power transfer function, and that both of these converge to a result that is proportional to the total radiation efficiency and therefore can be used for measuring efficiency related quantities. The two processes are:

1. *The random NLOS mode stirring process* that is known from earlier work to create a complex Gaussian H_{21}^c contribution to S_{21}.
2. *The random LOS process* caused by the "stirred" direct coupling, i.e., we will assume that H_{21}^d is a process that is randomized by changing the AoA of the direct LOS contribution using rotate-able platform and multi-chamber-antenna (i.e., polarization) stirring.

We will herein simply assume that the latter direct coupling process is:

a) complex Gaussian in the same way as the NLOS stirring process;
b) a power average that is proportional to the total radiation efficiency of the AUT independent of the shape of its radiation pattern.

The latter assumption b) is known to be valid if we sample the radiation pattern of the AUT uniformly distributed over its surrounding unit sphere during the platform and polarization stirring. The former assumption a) will be valid if the AUT is a practical small antenna with irregular far field function, whereas it is not valid for small antennas with regular or directive far field functions such as incremental electric or magnetic sources and Huygen's sources, according to the studies in [18], [32]. Anyway, the assumptions are physically defendable, and we will see that the results become quite useful and are able to model the measurement uncertainties observed in practice.

The above two Gaussian processes are independent, and therefore we can estimate the total uncertainty in predicting the transferred power from a variance obtained by adding the variances associated by each process, according to statistic theory, which we do in (18) below. Note that the standard deviation is the square root of the variance around the average.

A. Random NLOS Process: Mechanical Stirring Bandwidth B_{mech} and Number of Independent Samples

The chamber transfer function in (6) is proportional to the radiation efficiency, independent of which antenna or terminal we use. This is true only if the mode stirring creates enough independent samples, and if the direct coupling can be neglected. The H_{21}^c samples are complex Gaussian distributed (for sufficient independent samples). Then, the relative accuracy by which we can estimate $G_{chamber}$ has a relative standard deviation of [4]

$$\sigma_{NLOS} = \frac{1}{\sqrt{N_{ind}}} \tag{9}$$

where N_{ind} is the number of independent samples, which is a frequency-dependent subset of the total number of samples, i.e., stirrer positions. This means that we need $N_{ind} = 100$ for an accuracy of $\pm 10\%$, i.e. ± 0.5 dB. Thus, it is crucial that we can obtain at least 100 independent samples by the mode stirring.

The number of independent samples is determined primarily by the number of excited modes, which is related to the mode density in the chamber, i.e., to the number of modes per MHz. The mode density is given to good approximation by the classical formula (commonly referred to as Weyle's formula, see [8])

$$\frac{\partial N_{\text{mode}}}{\partial f} = \frac{V f^2 8\pi}{c^3}. \tag{10}$$

We choose to express the number of excited modes as

$$N_{\text{mode}} = \left\{ \frac{\partial N_{\text{mode}}}{\partial f} \right\} (B_{mech} + \Delta f) \tag{11}$$

where B_{mech} is a mechanical mode stirring bandwidth and Δf is the average mode bandwidth. B_{mech} is then a measure of how much the stirrers are able to change the resonance frequencies of the modes in the cavity, not only recombining existing modes with different excitations. B_{mech} has not yet been studied in detail, but it is believed to be quite insensitive to chamber loading and to frequency variations over large frequency ranges, whereas it depends on mode stirring methods and sequences, mechanical stirrer shapes, and chamber shape (at least for small chambers). The question is now how the number of independent samples is related to the number of excited modes. It is clear that it is many times larger than that, and there are several possible hypothesis such as e.g., that it has a maximum available value equal to the number of excited plane waves in the chamber, and this is according to [5] with quite good accuracy given as eight times the number of modes excited. However, it may even be larger. We use in the present paper the following simplified formula

$$N_{ind} = M_{plate} M_{pf,ind} M_{ant} \tag{12}$$

with M_{plate} equal to the number of plate positions, $M_{pf,ind}$ the number of independent platform positions, and M_{ant} the number of antennas used for the polarization (or multi-probe) stirring. Thus, the formula does not contain N_{mode} and thereby not B_{mech} because we found that we do not have enough plate positions for N_{mode} to represent any bounds, not even at the low frequencies. B_{mech} seemed though to be in the order of 4.5 MHz for the RTS chamber and 2.5 MHz for the HP chamber, but we will return to this in a later paper by a separate and careful study of this in which B_{mech} is determined by the value that makes the theory coincide in least square sense with measured uncertainties.

The number of platform positions must be bounded by the correlation distance between neighboring antenna positions. This should be in the order of 0.5 wavelengths, but we should even have an effect of the platform when the antenna is located

at the center of the platform. We model these two effects by using the following formula

$$M_{pf,ind} = \max \left\{ 8, \min \left[M_{pf}, \frac{2R \sin \left(\frac{2\pi}{M_{pf}} \right) M_{pf}}{\frac{\alpha \lambda}{2}} \right] \right\}$$
(12b)

which is an extension of the formula introduced in [33], where $\min(\bullet)$ and $\max(\bullet)$ are functions choosing the minimum and maximum, respectively, of the two arguments. M_{pf} is the number of platform positions, and R is the radius of the circle that the phase center of the AUT follows when the platform rotates. The factor α was varied to see when (12b) gave the best results, and it turned out to be approximately when $\alpha = 0.7$. Thus, we assume by using (12b) that two platform positions are independent when the phase center of the antenna has moved more than $0.7 \times 0.5 = 0.35$ wavelengths λ, and the number 8 in the formula makes sure that this value cannot be smaller than 8. Thus, if $R = 0$, so that the platform stirring corresponds entirely to a rotation of the antenna and no displacement, there can still be 8 independent platform positions. This corresponds to being able to resolve the 8 incident waves of each mode.

The same formula could be applied to the chamber antennas, but they are mounted far away from each other (in HP chamber) and have orthogonal orientations (in both HP and RTS chambers), so they can be considered uncorrelated so there is no bound on M_{ant} in (12b).

B. Random LOS Process: Approximation of Rician K-Factor

The reverberation chamber can be loaded to emulate multi-path propagation environments with different coherence bandwidths, see Table I. The load will reduce the statistic chamber contribution in (6) whereas the deterministic direct coupling in (5) will be unaffected (provided the loads are not blocking the line of sight between the two antennas). Thereby, loading can be used to emulate a Rician fading distribution of the received voltage with different K-factors.

The amount of direct coupling can therefore very conveniently be quantified by means of the Rician K-factor, i.e., the power of the LOS component relative to the average power of the statistic chamber contribution. Thus, by using Hill's and Friis' transmission formulas in (6) and (5), respectively, the Rician K-factor becomes (this equation is also derived in [7] without using Hill's transmission formula, but in a more lengthy way than here)

$$K = \frac{\left| H_{21}^d \right|^2}{\left| H_{21}^c \right|^2} = \frac{V}{r^2} \frac{\Delta f}{c} D_t D_r$$
(13)

in which we have used that the realized gains of the chamber antenna and the DUT are

$$G_1 = e_{rad1} D_1 \quad \text{and} \quad G_2 = e_{rad2} D_2,$$
(14)

respectively, with D_1 and D_2 their directivities in the directions of each other. V, c and Δf in (13) are the same as in (6). Equations (13)–(14) can be used to estimate the K-factor if the directivities of the antennas are known, or can be estimated. We see that K increases linearly with the average mode bandwidth

Δf. Thus, the greater the loading, the larger the Rician K-factor becomes.

We consider here only the case when direct coupling is undesirable, and therefore we want to reduce D_1 and D_2. Then, the chamber antenna should be a low gain antenna, or it can be pointed towards a wall or corner of the chamber, or towards a mechanical stirrer. Furthermore, the reference antenna for calibration, the AUT and the antenna of the DUT should be small antennas with low directivities as well. The maximum theoretical directivity of a small antenna is 4.8 dBi [34], achievable with a Huygen's source.

C. Random LOS Process: Evaluation of Average K-Factor, and Stirring Using Multiple AoA

By studying direct coupling using (13) in a reverberation chamber with low-gain antennas, it was found that the K-factor varies with frequency, as well as position and orientation of the AUT on the rotate-able platform. This is natural because the AUT and the chamber antenna will change their mutual orientation. The direct LOS coupling will change with platform position. Therefore, it is relevant to characterize the direct coupling in terms of an average K-factor, considering an arbitrary location of the AUT or DUT in the chamber. Such average K can be estimated using average values of $1/r^2$, D_1 and D_2. The average K-factor can also easily be determined from the measured S_{21} during calibration of the chamber, as explained in detail in [35]. Such evaluation of the average K-factor has been done for several different loadings and will be presented in Section VII.

We have initially in the beginning of Section V assumed that the random LOS process caused by platform and polarization stirring is Gaussian. Therefore, the uncertainty by which we can estimate the average power level of the random LOS contribution, is

$$\sigma_{LOS} = \frac{1}{\sqrt{M_{LOS,ind}}}$$
(15)

where $M_{LOS,ind}$ is the number of independent samples of all M_{LOS} platform and chamber antenna samples. We have investigated if the number of platform positions in (16) has similar bounds as for the NLOS component in (12b), but we were not able to observe such bounds for the choice of parameter variations in our measurements. The best agreement with measured uncertainties was obtained when

$$M_{LOS,ind} = M_{pf} M_{ant,ind}$$
(16)

where $M_{ant,ind}$ is the number of independent chamber antennas for the LOS case, i.e.,

$$M_{ant,ind} = \begin{cases} 3 & \text{for HP chamber} \\ 1 & \text{for RTS chamber} \end{cases}.$$
(17)

$M_{ant,ind} = M_{ant}$ when the chamber antennas are separated so much that the AoA to the AUT is considerably different for each chamber antenna. The three chamber antennas are located on orthogonal walls in the HP chamber, so the number is three, whereas they are co-located in the RTS chamber so that the AoA is the same for all chamber antennas, and thus there is only one independent LOS chamber antenna case. We have in Fig. 9 included results showing that the chamber antennas actually do

not stir the LOS contribution in the RTS chamber, but the uncertainty of the RTS chamber is still better than the HP chamber.

D. Combined Measurement Uncertainty Formula

The combined measurement uncertainty is now a result of combining the uncertainties of the two independent Gaussian processes, the random NLOS process and the random LOS process, according to the discussion in the beginning of Section V. This can be done using basic statistical theory, and gives by using (9) and (15) a combined relative standard deviation (STD) of

$$\sigma = \frac{\sqrt{(\sigma_{NLOS})^2 + K_{av}^2 (\sigma_{LOS})^2}}{\sqrt{1 + K_{av}^2}}. \tag{18}$$

In the present paper, the STD σ is presented in dB scale by averaging the dB values of $(1 + \sigma)$ and $(1 - \sigma)$, i.e.,

$$\sigma_{dB} = \frac{10\{\log(1 + \sigma) - \log(1 - \sigma)\}}{2} = 5\log\left(\frac{1 + \sigma}{1 - \sigma}\right). \tag{19}$$

The agreement with evaluated standard deviations for a practical chamber in Section VII shows that (18) is valid and useful.

VI. PROCEDURE FOR CALIBRATION AND ASSESSMENT OF UNCERTAINTY OF SPECIFIC CHAMBER

The purpose of calibrating a reverberation chamber is to obtain a reference value for the average power transfer function. This is normally done by the measurement set-up in Fig. 2 using a VNA. The reference antenna must have known total radiation efficiency, and it should be non-directive in order to be as similar as possible to the small antennas used in wireless devices. We will here use a wideband disk-cone antenna provided by Bluetest AB. The disk-cone has, when it is oriented vertically, vertical polarization and omnidirectional radiation in the horizontal plane. The reflection *coefficient* S_{11} of the disk-cone used here was better than $-10\,\text{dB}$ between 0.6 and 7 GHz when measured in free space.

A. How to Determine Reference Transfer Function (G_{ref})

The reference transfer function of a reverberation chamber is the power transfer function averaged over a full stirring sequence, and it is used as a reference for all passive (efficiency, diversity gain, MIMO capacity) and active (TRP, receiver sensitivity, throughput) measurements, in order to account for the average path loss in the chamber between the ports of the transmit antenna and the ports of the receive antenna. The reference transfer function is calculated from the measured S-parameters of the chamber by using

$$G_{ref} = \frac{\overline{|S_{21}|^2}}{e_{ref}} \tag{20}$$

where e_{ref} is the total radiation efficiency of the reference antenna, and $\overline{|S_{21}|^2}$ is a compact way of writing the average of

$\overline{|S_{21}|^2}$ over all stirrer positions as before. If the antenna is lossless, the total radiation efficiency is equal to the mismatch factor which can be computed from the measured S_{22} using (2) and

$$e_{ref} = 1 - |\overline{S_{22}}|^2. \tag{21}$$

We can also use the value for the free space S-parameter measured e.g., in an anechoic chamber in order to determine e_{ref}. This is advantageous because reflection-type S-parameters can be measured more accurately in an anechoic chamber than extracting them from measurements in reverberation chamber using (2).

The mismatch of the chamber antennas is not removed by calibration in (20), because this will be present in the same way also during measurements. However, in order to compute the average mode bandwidth accurately we need to correct for it, and define a net average power transfer function by

$$G_{ref,net} = \frac{(\overline{|S_{21}|^2})}{(e_{totrad} \cdot e_{ref})}. \tag{22}$$

When we use three (generally $M_{ant.}$) chamber antennas, they may be a bit different, and we can compute an average net reference transfer function from

$$G_{ref,net} = \frac{1}{M_{ant}} \sum_{j=1}^{M_{ant}} \left[\frac{\overline{|S_{21}|^2}_j}{e_{radj}} \right] \cdot \frac{1}{e_{ref}}. \tag{23}$$

It is important to be aware that we during calibration and passive measurements have access to complex S-parameters, which we do not have during active measurements. Therefore, we cannot make advanced processing of the S-parameters in order to produce a better reference level. We may e.g., not remove the direct coupling from the reference transfer function by using (4).

B. How to Determine Theoretical Uncertainty

We need to determine the average Rician K-factor in order to use the new theoretical model for the uncertainty given by (18). We may also need to determine the average mode bandwidth Δf if we introduce the bounds on N_{ind} given by (11), but as discussed there this has not been used in the present paper.

The average Rician K-factor is readily from a calibration measurement as explained in [35]. We will compute it in that way. It is also possible to estimate it using (13) if there is LOS between the antennas.

Mode bandwidth is defined as the bandwidth over which the excited power in a particular cavity mode with resonance frequency f_0 is larger than half the excited power at f_0. The average mode bandwidth Δf is the average of the mode bandwidths of all the modes excited at a certain frequency f, and it is related to the reference transfer function by (6). This means that it can be used as a measure of the attenuation through the chamber.

The average mode bandwidth can be calculated from (6) as expressed in [35], i.e., from

$$\Delta f = \frac{c^3}{16\pi^2 V f^2 G_{ref,net}} \qquad (24)$$

where c is the speed of light, V the inner volume of the chamber cavity, f the test frequency, and $G_{ref,net}$ the net reference transfer function of the chamber in either (22) or (23).

The average mode bandwidth can alternatively be determined from the coherence bandwidth in (26).

C. Procedure for Assessment of Uncertainty

The uncertainty can be assessed by repeating the calibration procedure several times for different positions and orientations of the reference antenna inside the reverberation chamber. We will here locate the reference antenna at three different heights on the rotate-able platform, and we will orient it in three directions, i.e., vertically, horizontally and at 45 deg relative to the vertical. (The orthogonal horizontal polarization is automatically covered by the rotating platform, so that a horizontally polarized reference antenna actually will have different polarizations at all platform positions.) Thereby, we will make in total 9 calibrations to assess the measurement uncertainty, and each calibration will give a reference transfer function according to (20). We will compute the standard deviation of the 9 reference transfer functions relative to the average of them, where the average is a good estimate of the expected true value. The number 9 is chosen as a compromise between acquisition time and uncertainty of the STD estimate. The relative uncertainty by which we can estimate the STD is only 1/3 if we have 9 independent measurement sequences. However, we will also smoothen the square of the STD over 50 MHz, and this will improve the uncertainty because the measurements at frequencies separated by more than the coherence bandwidth (i.e., the average mode bandwidth) can be regarded as uncorrelated, and thus independent. Therefore, we will for load0 and load1 cases improve the uncertainty by a factor of the square root of 25, i.e., 5. The number 25 is explained by taking the 50 MHz divided by a coherence bandwidth of about 2 MHz according to Fig. 4. Thus, the total uncertainty of the estimation of STD will be about $1/(3 * 5) = 7\%$, and we will be satisfied with this.

D. Polarization Imbalance – A Systematic Uncertainty

The K-factor will represent a systematic error in the results, but the effect of it can be reduced by polarization or platform stirring as seen from the uncertainty formula. There may also be a systematic error if only either TE- or TM chamber modes are excited in the chamber. Both an unstirred K-factor and an unstirred systematic mode excitation error may cause a polarization imbalance, i.e., that the average power transfer function depends on the orientation of a linearly polarized antenna inside the chamber. The latter mode excitation error may appear if the chamber and its mechanical stirrers are too regularly shaped, i.e., too rectangular, so that TE- and TM-modes do not mix when stirred. Such polarization imbalance will be removed by polarization stirring using several orthogonal chamber antennas [22].
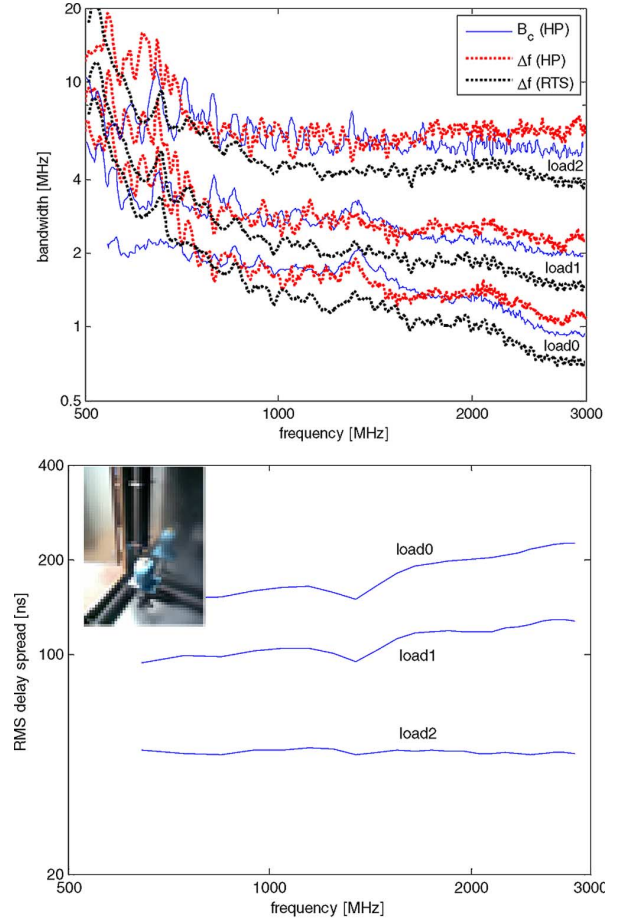

Fig. 4. Average mode bandwidths and coherence bandwidths (upper graph) of both HP and RTS Bluetest chambers, and RMS delay spreads (lower graph) of the HP chamber, for the three different loads defined in Table II. The inserted photo shows the load2 configuration with a head phantom and three lossy cylinders along three orthogonal corners between walls. The RMS delay spread is computed from the frequency data of S_{21} by using a wideband FFT. Therefore, there are missing frequency points at the beginning and end of the delay spread curves. The RMS delay spread results were produced only from HP chamber data for which we had closer frequency points.

The polarization imbalance can be quantified in the following way based on several measurements of vertically and horizontally polarized antennas in the chamber. We consider 3 orthogonal polarizations of the reference antenna, i.e., $polref = 1, 2, 3$. For each of these polarizations we measure the average power transfer function N_{pol} times. We create a reference level by averaging over all 3 polarizations, and then the polarization imbalance of each polarization $polref$ with respect to this reference level becomes

$$\frac{P_{polref}}{P_{ref}} = \frac{\frac{1}{N_{pol}} \sum_{ipol}^{N_{pol}} P_{ipol}}{\left\{ \frac{1}{3} \sum_{polref=1}^{3} P_{polref} \right\}} \qquad (25)$$

where P_{ipol} is the average power transfer function for several measurements of each polarization of the reference antenna in N_{pol} different positions, respectively.

E. How to Determine Coherence Bandwidth

For measurements of throughput and receiver sensitivity the coherence bandwidth is of interest, because system performance is affected by coherence bandwidth and time delay spread.

It is physically obvious that the average mode bandwidth must be proportional to the coherence bandwidth inside the chamber, and in [19] it is shown that they actually are equal if the coherence bandwidth is defined as the bandwidth over which the complex correlation function has decreased from 1 to 0.5, i.e., then

$$B_{coherence} = \Delta f. \qquad (26)$$

The average RMS delay spread is in the reverberation chamber related to the coherence bandwidth by[19]

$$\sigma_\tau = \frac{1}{(2\pi\sqrt{3}B_{coherence})}. \qquad (27)$$

Alternatively, the coherence bandwidth can be determined from the complex autocorrelation function (see e.g., [36] for the relation between envelop correlation function and complex correlation function), i.e.,

$$\rho_f(\partial f) = \left| \frac{S_{21}^{c}{}^{*}(f) \cdot S_{21}^{c}(f + \partial f)}{|S_{21}^{c}(f)|^2} \right| \qquad (28)$$

where the averaging is taken over all stirrer positions. (We can get a more clear (unique) correlation function by evaluating it for each chamber antenna and platform position using the statistic chamber contribution H_{21}^{c}.) The coherence bandwidth $B_{coherence}$ is the half bandwidth at which the value of the complex autocorrelation function is 0.5.

F. Power-Delay-Profile

The time domain behavior of a signal propagating within the chamber is described by the power delay profile (PDP). It shows the power amplitude at the receiver as a function of time for a transmitted pulse, and is commonly used to characterize real multipath environments. The PDP is normally considered to be the average delay profile over a certain amount of time, which in the reverberation chamber corresponds to the average delay profile over a complete stirring sequence. The PDP is important for determining how digital receivers of modern wireless systems will perform in a specific environment.

PDP's are normally measured by synthesized pulsing, i.e., the frequency response of the chamber is measured over a certain bandwidth and then inverse-Fourier transformed to achieve the time response. The data from a calibration measurement can with advantage be used for this, if the data for each sweep have been saved during the measurement process. More details about calculating PDP's from the chamber S-parameters are found in [19]. This is much easier than to determine it from actual time delay measurements.

The PDP in reverberation chambers are normally exponentially shaped, with a high number of incoming signals, i.e., a rich scattering environment. Since the shape of the PDP is supposed to be very similar from chamber to chamber, there are simpler

TABLE II
DEFINITION OF CHAMBER, STIRRING SEQUENCES AND LOADS. THE PVC CYLINDERS WERE FILLED WITH MICROWAVE ABSORBERS CUT IN SMALL PIECES AND PRESSED MANUALLY INTO THE CYLINDERS

Parameter	Definition
Chamber size	1.8 m × 1.7 m × 1.2 m
Mechanical plate stirrers	2 as defined in Section II. Simultaneous movements to 50 for HP and 25 for RTS equally spaced positions.
Radius on platform	Antennas located with R = 10 cm. 20 equally spaced positions.
Chamber antennas	HP: 3 located at ceiling and two orthogonal walls. RTS: 3 located on a cube behind a shield.
Total number of samples	3 chamber antennas × 20 platform positions × 50 (or 25) plate positions
Load0	No loads, except for 3 chamber antennas, 1 more antenna for other purposes, and reference antenna.
Load1	Same as empty, and additional head phantom
Load2	Same as load 1, and additional 3 lossy PVC cylinders located as shown in Figure 5.

parameters to use for describing the time domain behavior, e.g., the RMS delay spread in Fig. 4.

VII. RESULTS FOR CHAMBERS IN SECTION II

We will here present results for the Bluetest HP and RTS chambers described in Section II. The RTS chamber is a modified HP chamber, done as part of the present study.

The first modification of the chamber addressed the stirred volume of the plate stirrers, and the premise that the number of independent samples increases if the stirred volume increases. This should increase B_{mech} in the model in (11). Thus, the width of the metallic plates was increased; the dimensions are given in Section II. The stirred volume in the traditional chamber is 13.8% of the total chamber volume, whereas the chamber with improved stirring configuration has a stirred volume of 22.4% of the total chamber volume. We have already mentioned after (12) that we observed an improvement in B_{mech}, but this is not so significant for the results presented because we need more plate positions. Therefore, we will leave the study of B_{mech} for a future paper.

The second modification addressed the premise that the K-factor affects the accuracy of the measurements. In order to decrease this parameter further, the chamber antennas were removed from the walls and placed on three orthogonal sides of a metal cube that was located on a vertical PVC support tube standing on the chamber floor behind a shielding plate. This completely removes the LOS contribution between the transmitting and the receiving antennas, but there may still be some diffraction contribution above the edge of the shield or reflection via the closest wall.

The stirring sequences and chamber loads are defined in Table II. The S-parameters of the chamber were measured with a frequency step of 1 MHz between 500 MHz and 3 GHz. For the RTS chamber we used 2 MHz frequency step.

Fig. 4 shows computed results for the average mode bandwidth Δf using (24), coherence bandwidth $B_{coherence}$ using (28), and average delay spread as explained in Section VI.F, for the four different loads. The curves for both Δf and $B_{coherence}$ were smoothened by averaging over a 20 MHz window before
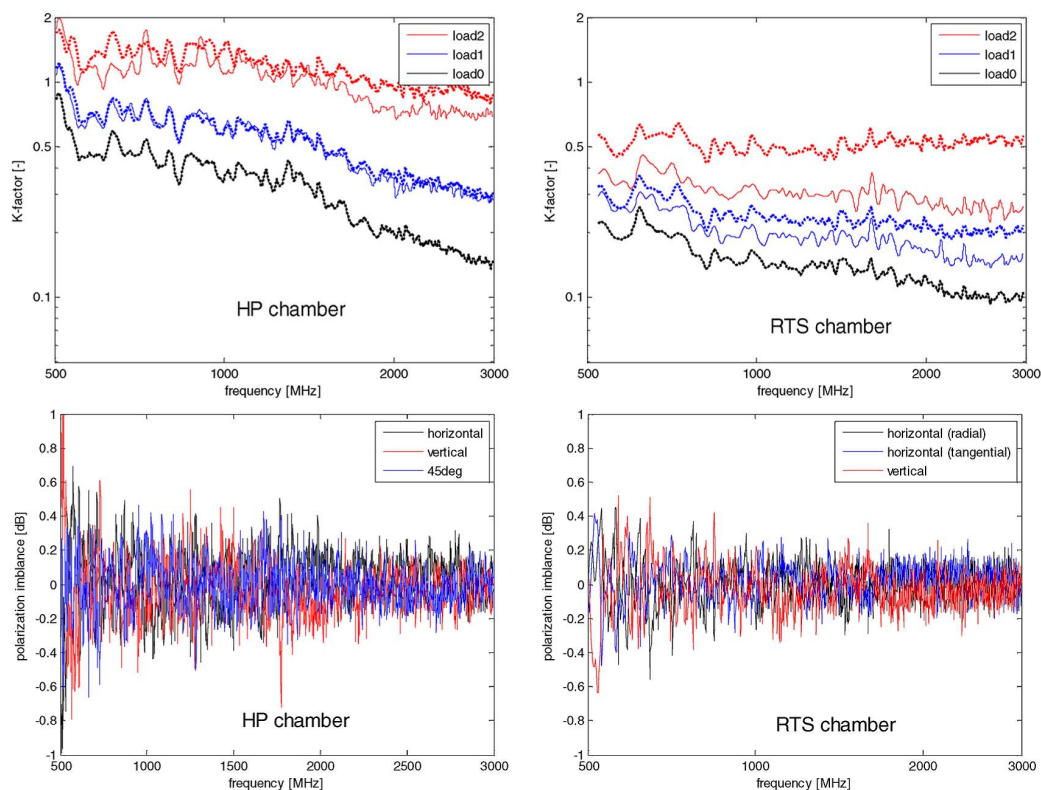
Fig. 5. Average Rician K-factor (upper) and polarization balance (lower) calculated as described in the text from measured S-parameters from Bluetest HP reverberation chamber (left) and RTS60 reverberation chamber (right). The solid curves in the K-factor graphs are calculated directly from (17), whereas the dotted curves are calculated by using the average K-factor for the $load0$ case, and scaling it by the factors $\Delta f_{load1}/\Delta f_{load0}$ and $\Delta f_{load2}/\Delta f_{load0}$ for the $load1$ and $load2$ cases, respectively, by using their proportionality to average mode bandwidth in (13). The polarization balance is for the $load0$ case.
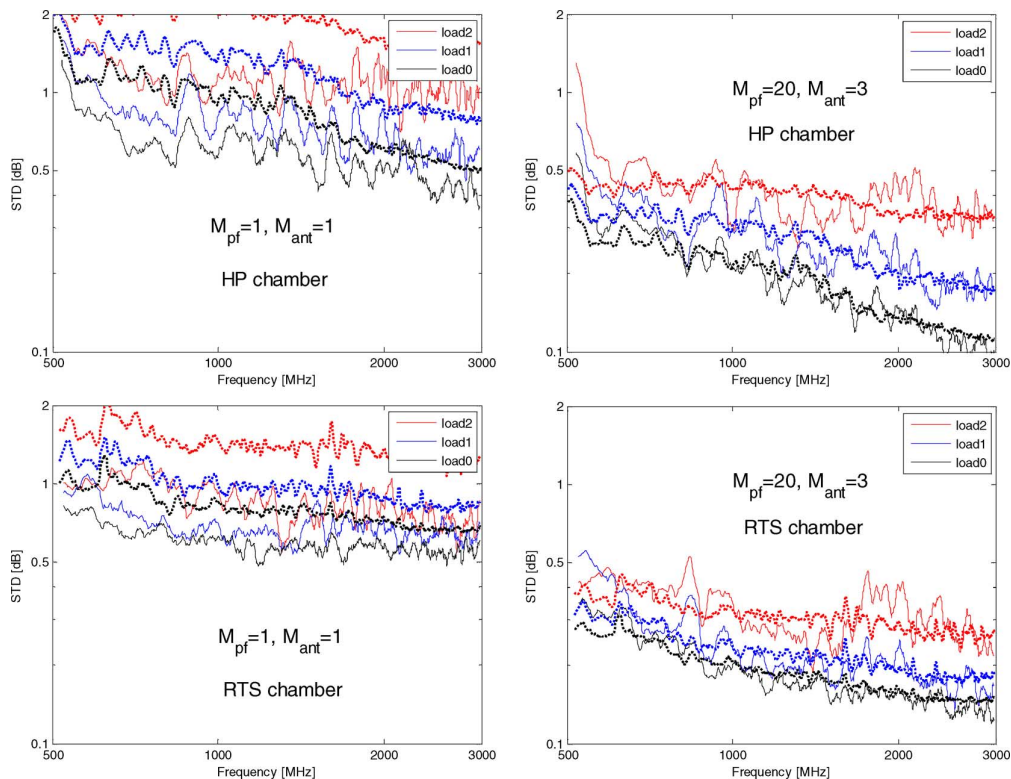

Fig. 6. Standard deviations of the Bluetest HP chamber (upper graphs) and RTS chamber (lower graphs) calculated from nine calibration measurements of the average power transfer function (solid line), and for comparison theoretical curves (dotted lines) calculated from the above formulas using the measured average K-factors in Fig. 4. The left graphs are without and the right graphs with platform and polarization stirring, as given by the values of M_{pf} and M_{ant} .
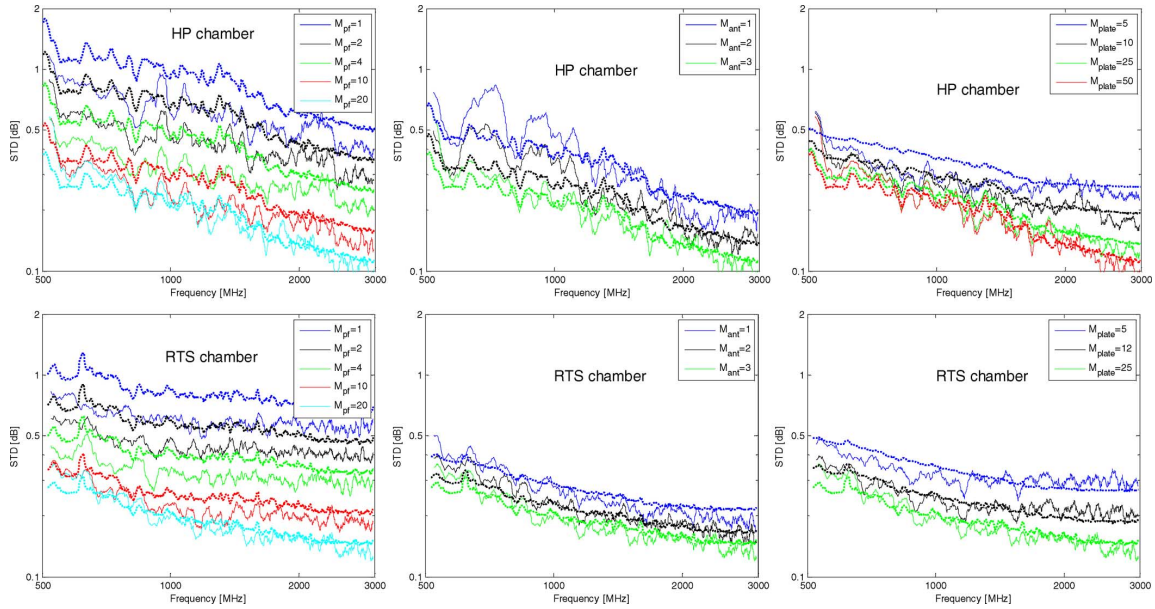
Fig. 7. Standard deviations of the Bluetest HP chamber (upper graphs) and RTS chamber (lower graphs) calculated from nine calibration measurements of the average power transfer function (solid line), and for comparison theoretical curves (dotted lines) calculated from the above formulas using the measured average K-factors in Fig. 4. The graphs show variation of STD with different number of platform positions (left graphs), number of chamber antennas (middle graphs), and number of plate positions (right graphs). The numbers of positions of the two other stirring methods (that are not varied within a graph) have their maximum values.

they were plotted. We see that the average mode bandwidth and the coherence bandwidth are nearly equal in size. The Δfs of the two chambers are very similar.

The average Rician K-factor was determined for both chambers as explained in [35], and an additional averaging over the 9 calibration cases. The K-factor still varied a lot with frequency, so therefore we smoothened it over a floating 20 MHz window before plotting, for clarity. It is presented in Fig. 5 for the three different loads. We see that the K-factor increases strongly with the loading as expected, and that it is much lower for the new RTS chamber than the old HP chamber, as a result of the improvements. The dotted curves show average K-factors calculated from the K-factor for the load0 case by using the proportionality with the average mode bandwidth Δf in (13). We see that clearly this proportionality is present in the HP chamber that has a clear LOS between the chamber antennas and the AUT, but not in the RTS chamber where the chamber antennas have been hidden behind a shield. The same figure shows the polarization imbalance. We see that it is small over the whole frequency range, mainly due to the polarization stirring, and also that it is significantly better for the new RTS chamber. There is no systematic difference between the results for the three orientations of the reference antenna.

A. Uncertainty for Stepwise Stirring

The total measurement uncertainties for both chambers are plotted side-by-side in Fig. 6, for different parameter variations of the stirrers, i.e., number of plate, platform and chamber antennas, and for the three loads. The solid lines show standard deviations calculated from nine calibration measurements of the average transfer function by using the average of these nine

measurements as the correct value, as explained in Section VI. The final standard deviation was smoothed over 20 MHz before being plotted. For comparison, we show theoretical curves as dotted lines. These have been calculated as explained in Section VI using the measured average K-factors in Fig. 4.

We see that the theoretical STD curves describe the main characteristics of the measured STDs very well, from only knowledge of the average K-factor and mechanical parameters of the stirring. The upper and lower graphs show cases without and with platform and polarization stirring, respectively. We see very clearly from the results that the platform and polarization stirrings have very strong effect on the uncertainties, and are the most important of all the stirring methods to achieve good accuracy. We also see that the empty chamber, and the chamber loaded with a head phantom (load1) give much better accuracy than the other more heavily loaded cases.

Fig. 7 shows how sensitive the STD is to decreasing the number of platform positions, chamber antennas, and plate positions. These curves were obtained from the measured data samples by selecting every second, third or fourth of the collected samples. We see that in all cases the agreement between theory and measurements are very good, in particular for the cases with many stirrer positions and for small loads.

The uncertainties of the two chambers are compared in the same graphs in Fig. 8, for all three loads. The improvement of the improved RTS chamber is clearly observed.

To address the effect of the co-located chamber antenna on $M_{ant,ind}$ in (17), and therefore on the uncertainty of the RTS chamber, we plot in Fig. 9 the theoretical curves obtained by using $M_{ant,ind} = 3$, to be compared with the lower right graph in Fig. 6. We see that the theoretical curves obtained by using $M_{ant,ind} = 1$ shows much better agreement with the measured

Fig. 9. The STDs of the RTS chamber (solid line) and the "wrong" theoretical curves (dotted lines) calculated using (19) but with $M_{ant,ind} = 3$ instead of 1.
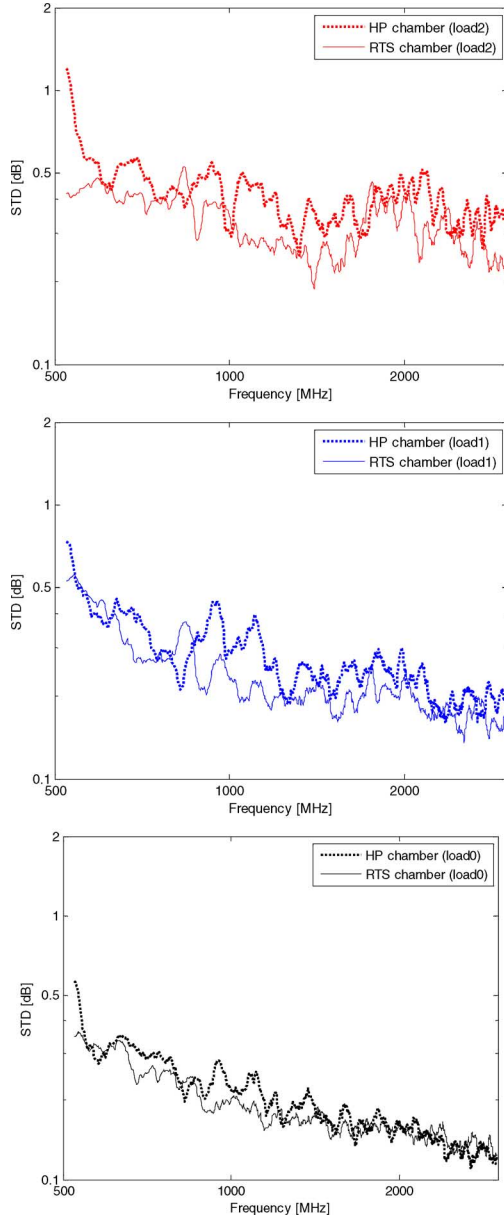

Fig. 8. The STD calculated from 9 calibration measurements for the original Bluetest HP reverberation chamber (dotted lines) and the improved RTS chamber (solid lines), both by using a stepwise stirring as explained in the text. Note that for fair comparison, we used 25 plate positions for both chambers even if we had data for 50 plate positions available for the HP chamber. The number of platform positions is 20, and the number of chamber antennas is 3.

Fig. 10. The STD calculated from 9 calibration measurements for the HP chamber (upper) and the improved RTS chamber (lower), both by using fast continuous stirring. The red curve shows the STD smoothened over a 50 MHz bandwidth.

curves than the theoretical curves in Fig. 9. This confirms our physical LOS stirring hypothesis also for the RTS case.

B. Uncertainty for Continuous Stirring

We also performed the nine calibration measurements by using continuous stirring, which is much faster.

The results of these can be studied in Fig. 10, both for the HP and RTS chambers. We see in this case a more clear improvement of the RTS chamber compared to the original HP chamber. The Fig. shows that the mean STD has decreased to between 0.2 and 0.3 dB over the entire frequency range of interest. It can also be seen that the statistical fluctuations have decreased, and that
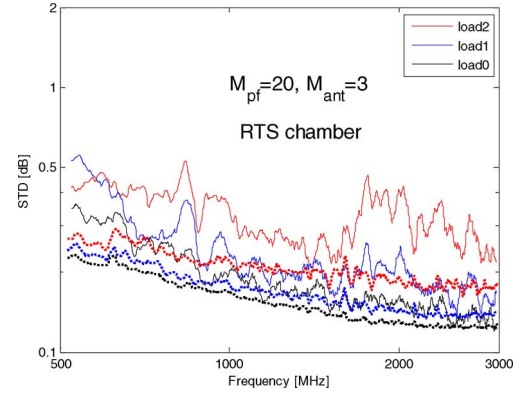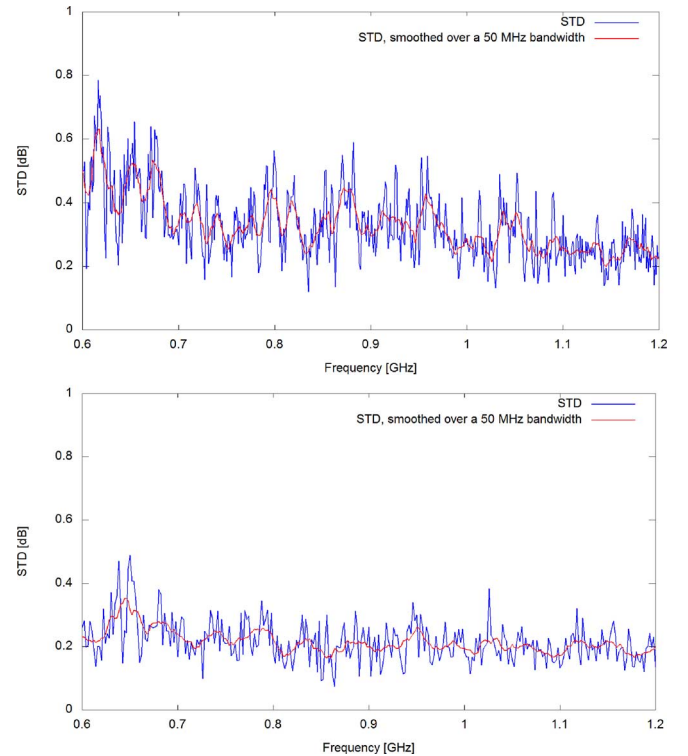
there are no peaks above 0.5 dB. The reason for this may be that the continuous stirring is asynchronous, so that the mechanical stirrers may pass through more independent positions than in the discrete stirring case.

Table III shows a comparison of the STD between the original chamber and the improved one with the new stirring configuration. The maximum STD in a given frequency interval is also given. The table shows clearly the improvement of the measurement accuracy by improving the chamber.

The STD could be reduced even more, because at high frequency it is limited by the number of collected samples. However, to gather more samples the measurement time will increase, and therefore it is not motivated.

TABLE III
MAXIMUM MEAN STANDARD DEVIATION IN DIFFERENT FREQUENCY
INTERVALS FOR THE REVERBERATION CHAMBER DESCRIBED IN SECTION II
(BLUETEST HP CHAMBER) AND THE SAME WITH IMPROVED STIRRING
CONFIGURATION (RTS60 CHAMBER)

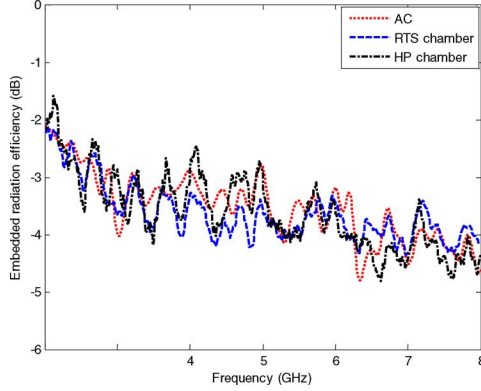| Frequency interval [37]	Bluetest HP chamber		Improved RTS60 chamber	
	Mean STD	Max STD	Mean STD	Max STD
$0.6 - 0.7$ GHz	0.55 dB	0.82 dB	0.31 dB	0.49 dB
$0.7 - 1.0$ GHz	0.35 dB	0.55 dB	0.25 dB	0.38 dB
$1.2 - 6.0$ GHz	0.30 dB	-	0.20 dB	-

Fig. 11. Embedded radiation efficiency at the differential port of 180° (lossy) hybrid connecting to one petal of Eleven antenna.

VIII. EXAMPLE

To illustrate the general study of uncertainty and the improvement of the RTS chamber, we measured the efficiency of a wideband log-periodic folded dipole array, the so-called eleven antenna described in [38] and designed for the frequency range 2–13 GHz. The measurements were first done in the anechoic chamber (AC) at Technical University of Denmark (DTU), and in the HP chamber at Chalmers, from 2 to 8 GHz as explained in [39], and thereafter for the purpose of the present paper we performed measurements also in the RTS chamber. In the reverberation chamber measurements we generated a reference level using a single frequency scan with the same disk-cone antenna used for the uncertainty study in Section VII. The average reference power level as well as the average power level with the eleven antenna were post-processed with 20-MHz frequency stirring. We gathered 600 samples per frequency, i.e., 20 platform positions, 10 plate positions (with the two plate moving simultaneously), and 3 chamber antennas, and the chambers were loaded with a head phantom, i.e., load1 case. The efficiency of the disk-cone reference antennas was achieved by measuring the losses of a cable equally long as the feeding cable built into it, and by using a mismatch factor obtained from measuring the free space S_{11}. In the anechoic chamber measurements a standard gain horn was used, and the efficiency was found as the ratio between the realized gain and the directivity.

The results in Fig. 11 show the embedded radiation efficiency measured at the differential port of the 180° hybrid connecting to one petal of the eleven antenna (see [39, Fig. 2]). Thus, this efficiency is low because it includes the effect of the so-called decoupling efficiency [40] between two opposing eleven antenna

petals as well as the losses in the 180° hybrid. We see from Fig. 11 that the efficiencies measured in anechoic chambers and in reverberation chambers are in very good agreement. To examine the discrepancy we calculated the STD of the difference between the efficiencies measured in each of the reverberation chambers and that measured in the anechoic chamber (AC). The STD of the efficiency difference between AC and RTS chamber is 0.35 dB and the STD between the AC and HP chamber is 0.38 dB. The expected value will depend on the uncertainty of the anechoic chamber, which is claimed to be 0.2 dB [39]. We also have to consider that the uncertainty of the reverberation chamber results is a factor $\sqrt{2} = 1.4$ larger than the level of 0.2 dB read from Fig. 8(b), because we have the same error associated with predicting both the reference level and the AUT level. If we add all these errors together as independent contributions we get a value of $\sqrt{3} \cdot 0.2$ dB $= 0.35$ dB which is very close to the actual measured deviation between AC and reverberation chambers.

IX. CONCLUSION

We have reformulated the transmission function through a reverberation chamber in a way that makes it easily recognizable for wireless propagation and system specialists. In this reformulation Friis' transmission formula describes the direct coupling between the transmitting and receiving antennas, corresponding to a LOS component, and Hill's transmission formula for reverberation chambers describes the averaged received power, corresponding to a multipath or NLOS contribution.

This new channel formulation has been used to derive a new expression for the uncertainty of efficiency-related measurements, such as radiation efficiency, total radiated power (TRP), total isotropic sensitivity (TIS) and throughput data rate. The main parameter of this uncertainty formula is the average K-factor of the chamber. This depends on the directivities of the fixed chamber antennas and their direct coupling to the AUT or DUT, but also on the loading of the chamber. It is shown to actually scale with the average mode bandwidth. The effect of the average K-factor can be strongly reduced by platform stirring and polarization (multi-probe) stirring. The STD contribution from the average K-factor is inversely proportional to the square root of the number of chamber antennas and platform positions.

The scaling of the K-factor with average mode bandwidth is also known from previous research [7]. However, we have found this not to be true for the RTS chamber where there is no LOS between the chamber antennas and the AUT. Still, even if there is no direct LOS, the K-factor model is shown to be valid and very useful for describing the uncertainty that is given by the same formulas as for the HP chamber having a LOS.

The investigations have resulted in an improvement of the stirring methods of the Bluetest reverberation chambers that was implemented in the new generation of RTS chambers. The main improvement was achieved by reducing the average K-factor by a factor between 0.5 and 0.7 by moving the chamber antennas behind a shield. The final STD of an unloaded chamber is below 0.2 dB over a significant part of the frequency band, and below 0.5 dB from approximately 550 MHz, in spite of the fact that the chamber is quite small with size 1.8 m × 1.7 m × 1.2 m.

The results show that after shielding of the direct LOS there is still is a small K-factor present in the RTS chamber. This may be caused by an unstirred field component in the form of a dominant mode, a major diffraction or reflection contribution, or similar. Anyway, the achieved uncertainty is still described very accurately by the average K-factor using the introduced uncertainty model. We have also shown that the co-location of the three chamber antennas of the RTS chamber causes that they have no effect on the stirring of the K-factor (apparent LOS component) Still, the RTS chamber is better than the HP chamber because of the shielding of direct LOS and the effective mode stirring of the NLOS chamber contribution.

The paper has introduced mechanical stirring bandwidth characterizing plate type stirrers, and a correlation distance of 0.35 wavelengths between uncorrelated samples of an antenna that is moved by platform stirring. The mechanical stirring bandwidth is at the end so large that it does not represent any bound on the number of independent plate positions, even though some additional studies not reported in the present paper indicate that it improved from around 2.5 MHz in the HP chamber to 4.5 MHz in the RTS chamber. This has to be studied more carefully later using more plate and platform positions.

The details of the new uncertainty model are tailored to the Bluetest chambers, but the ideas behind them are physical and general. Later, it would be interesting to go further down in frequency to determine the lowest frequency of operation, and to determine how high up in frequency the uncertainty models will work. Also, the two plate stirrers in the Bluetest are moved simultaneously to their positions. It would be interesting to see how the uncertainty improves if we move them independently to reach more combinations of positions. This could be a fact that can explain the better performance of the continuous stirring, because then the two plates are not moving in a synchronized way.

REFERENCES

[1] R. F. Harrington, *Time-Harmonic Electromagnetic Fields*. New York: McGraw-Hill, 1961.

[2] C.-T. Tai, *Dyadic Green Functions in Electromagnetic Theory*, 2nd ed. New York: IEEE Press, 1994.

[3] D. A. Hill, "Plane wave integral representation for fields in reverberation chambers," *IEEE Trans. Electromagn. Compat.*, vol. 40, pp. 209–217, 1998.

[4] J. G. Kostas and B. Boverie, "Statistical model for a mode-stirred chamber," *IEEE Trans. Electromagn. Compat.*, vol. 33, pp. 366–370, 1991.

[5] K. Rosengren and P. S. Kildal, "Study of distributions of modes and plane waves in reverberation chambers for the characterization of antennas in a multipath environment," *Microw. Opt. Technol. Lett.*, vol. 30, pp. 386–91, 2001.

[6] P. Corona, G. Ferrara, and M. Migliaccio, "Reverberating chamber electromagnetic field in presence of an unstirred component," *IEEE Trans. Electromagn. Compat.*, vol. 42, pp. 111–115, 2000.

[7] C. L. Holloway, D. A. Hill, J. M. Ladbury, P. F. Wilson, G. Koepke, and J. Coder, "On the use of reverberation chambers to simulate a Rician radio environment for the testing of wireless devices," *IEEE Trans. Antennas Propag.*, vol. 54, pp. 3167–3177, 2006.

[8] M. L. Bäckström, O. Lundén, and P. S. Kildal, "Reverberation chambers for EMC susceptibility and emission analyses," *Rev. Radio Sci.*, pp. 429–452, 1999.

[9] K. Rosengren, P. S. Kildal, C. Carlsson, and J. Carlsson, "Characterization of antennas for mobile and wireless terminals in reverberation chambers: Improved accuracy by platform stirring," *Microw. Opt. Technol. Lett.*, vol. 30, pp. 391–7, 2001.

[10] P. S. Kildal and K. Rosengren, "Correlation and capacity of MIMO systems and mutual coupling, radiation efficiency, and diversity gain of their antennas: Simulations and measurements in a reverberation chamber," *IEEE Commun. Ma.*, vol. 42, pp. 104–112, 2004.

[11] P. S. Kildal and K. Rosengren, "Electromagnetic analysis of effective and apparent diversity gain of two parallel dipoles," *IEEE Antennas Wireless Propag. Lett.*, vol. 2, pp. 9–13, 2003.

[12] P. S. Kildal, K. Rosengren, B. Joonho, and L. Juhyung, "Definition of effective diversity gain and how to measure it in a reverberation chamber," *Microw. Opt. Technol. Lett.*, vol. 34, pp. 56–9, 2002.

[13] K. Rosengren and P. S. Kildal, "Radiation efficiency, correlation, diversity gain and capacity of a six-monopole antenna array for a MIMO system: Theory, simulation and measurement in reverberation chamber," *IEEE Proc. Microw. Antennas Propag.*, vol. 152, pp. 7–16, 2005.

[14] C. Orlenius, P. S. Kildal, and G. Poilasne, "Measurements of total isotropic sensitivity and average fading sensitivity of CDMA phones in reverberation chamber," in *Proc. IEEE Antennas and Propagation Society Int. Symp.*, Jul. 3–8, 2005, vol. 1A, pp. 409–12.

[15] S. J. Floris, K. A. Remley, and C. L. Holloway, "Bit error rate measurements in reverberation chambers using real-time vector receivers," *IEEE Antennas Wireless Propag. Lett.*, vol. 9, pp. 619–622, 2010.

[16] E. Genender, C. L. Holloway, K. A. Remley, J. M. Ladbury, G. Koepke, and H. Garbe, "Simulating the multipath channel with a reverberation chamber: Application to bit error rate measurements," *IEEE Trans. Electromagn. Compat.*, vol. 52, pp. 766–777, 2010.

[17] P. S. Kildal, A. Hussain, X. Chen, C. Orlenius, A. Skårbratt, J. Åsberg, T. Svensson, and T. Eriksson, "Threshold receiver model for throughput of wireless devices with MIMO and frequency diversity measured in reverberation chamber," *IEEE Antennas Wireless Propag. Lett.*, vol. 10, pp. 1201–1204, Oct. 2011.

[18] P.-S. Kildal, C. Orlenius, and J. Carlsson, "OTA testing in multipath of antennas and wireless devices with MIMO and OFDM," *Proc. IEEE*, vol. 100, no. 7, pp. 2145–2157, Jul. 2012.

[19] X. Chen, P. S. Kildal, C. Orlenius, and J. Carlsson, "Channel sounding of loaded reverberation chamber for over-the-air testing of wireless devices: Coherence bandwidth versus average mode bandwidth and delay spread," *IEEE Antennas Wireless Propag. Lett.*, vol. 8, pp. 678–681, 2009.

[20] O. Delangre, P. De Doncker, M. Lienard, and P. Degauque, "Delay spread and coherence bandwidth in reverberation chamber," *Electron. Lett.*, vol. 44, pp. 328–329, 2008.

[21] Y. B. Karandikar, D. Nyberg, N. Jamaly, and P. S. Kildal, "Mode counting in rectangular, cylindrical, and spherical cavities with application to wireless measurements in reverberation chambers," *IEEE Trans. Electromagn. Compat.*, vol. 51, pp. 1044–1046, 2009.

[22] P. S. Kildal and C. Carlsson, "Detection of a polarization imbalance in reverberation chambers and how to remove it by polarization stirring when measuring antenna efficiencies," *Microw. Opt. Technol. Lett.*, vol. 34, pp. 145–9, 2002.

[23] P. S. Kildal, L. Sz-Hau, and C. Xiaoming, "Direct coupling as a residual error contribution during OTA measurements of wireless devices in reverberation chamber," in *Proc. IEEE Antennas and Propagation Society Int. Symp.*, 2009, pp. 1–4.

[24] P. Hallbjorner, U. Carlberg, K. Madsen, and J. Andersson, "Extracting electrical material parameters of electrically large dielectric objects from reverberation chamber measurements of absorption cross section," *IEEE Trans. Electromagn. Compat.*, vol. 47, pp. 291–303, 2005.

[25] D. A. Hill, M. T. Ma, A. R. Ondrejka, B. F. Riddle, M. L. Crawford, and R. T. Johnk, "Aperture excitation of electrically large, lossy cavities," *IEEE Trans. Electromagn. Compat.*, vol. 36, pp. 169–178, 1994.

[26] U. Carlberg, P. S. Kildal, and J. Carlsson, "Numerical study of position stirring and frequency stirring in a loaded reverberation chamber," *IEEE Trans. Electromagn. Compat.*, vol. 51, pp. 12–17, 2009.

[27] U. Carlberg, P. S. Kildal, and J. Carlsson, "Study of antennas in reverberation chamber using method of moments with cavity Green's function calculated by Ewald summation," *IEEE Trans. Electromagn. Compat.*, vol. 47, pp. 805–814, 2005.

[28] P. S. Kildal, C. Carlsson, and Y. Jian, "Measurement of free-space impedances of small antennas in reverberation chambers," *Microw. Opt. Technol. Lett.*, vol. 32, pp. 112–15, 2002.

[29] U. Carlberg, P. S. Kildal, A. Wolfgang, O. Sotoudeh, and C. Orlenius, "Calculated and measured absorption cross sections of lossy objects in reverberation chamber," *IEEE Trans. Electromagn. Compat.*, vol. 46, pp. 146–154, 2004.

[30] J. M. Ladbury and D. A. Hill, "Enhanced backscatter in a reverberation chamber: Inside every complex problem is a simple solution struggling to get out," in *Proc. IEEE Int. Symp. on Electromagnetic Compatibility*, 2007, pp. 1–5.

[31] A. Wolfgang, W. Carlsson, C. Orlenius, and P. S. Kildal, "Improved procedure for measuring efficiency of small antennas in reverberation chambers," in *Proc. IEEE Antennas and Propagation Society Int. Symp.*, 2003, vol. 4, pp. 727–730.

[32] P.-S. Kildal, U. Carlberg, and J. Carlsson, "Definition of antenna diversity gain in user-distributed 3D-random line-of-sight," *IEEE Antennas Wireless Propag. Lett.*, submitted for publication.

[33] A. Sorrentino, P. S. Kildal, U. Carlberg, and E. Pucci, "Accuracy in reverberation chamber for wireless testing: Simple formulas for the number of independent samples," in *Proc. 3rd Eur. Conf. Antennas and Propagation*, 2009, pp. 2673–2677.

[34] P. S. Kildal and S. R. Best, "Further investigations of fundamental directivity limitations of small antennas with and without ground planes," in *Proc. IEEE Antennas and Propagation Society Int. Symp. and USNC/URSI National Radio Science Meeting*, Piscataway, NJ, Jul. 5–12, 2008, p. 4.

[35] X. Chen, P. S. Kildal, and S. H. Lai, "Estimation of average Rician K-factor and average mode bandwidth in loaded reverberation chamber," *IEEE Antennas Wireless Propag. Lett.*, vol. 10, pp. 1437–1440, 2011.

[36] W. C. Jakes, *Microwave Mobile Communications*, 2nd ed. New York: Wiley, 1994.

[37] P. Hallbjörner, Z. Ying, M. Håkansson, C. Wingqvist, T. Anttila, and J. Welinder, "Multipath simulator for mobile terminal antenna characterisation," *IET Microw. Antennas Propag.*, vol. 4, pp. 743–750, 2010.

[38] J. Yang, M. Pantaleev, P. S. Kildal, B. Klein, Y. Karandikar, L. Helldner, N. Wadefalk, and C. Beaudoin, "Cryogenic 2–13 GHz eleven feed for reflector antennas in future wideband radio telescopes," *IEEE Trans. Antennas Propag.*, vol. 59, pp. 1918–1934, 2011.

[39] X. Chen, P. S. Kildal, J. Carlsson, and J. Yang, "Comparison of ergodic capacities from wideband MIMO antenna measurements in reverberation chamber and anechoic chamber," *IEEE Antennas Wireless Propag. Lett.*, vol. 10, pp. 446–449, 2011.

[40] M. V. Ivashina, M. Kehn, P. S. Kildal, and R. Maaskant, "Decoupling efficiency of a wideband Vivaldi focal plane array feeding a reflector antenna," *IEEE Trans. Antennas Propag.*, vol. 57, pp. 373–382, 2009.

surfaces from 1988, today being regarded as the first metamaterials concept. This concept is the basis of his newest and most fundamental invention, the gap waveguide technology. His research is innovative and industrially oriented, and has resulted in several patents and related spinoff companies, the most known being Bluetest AB (see www.kildal.se for more details). His textbook *Foundations of Antennas – A Unified Approach* (Lund, Sweden: Studentlitteratur, 2000) was well received, and is now in the process of being revised. He has authored more than 120 articles in scientific journals; concerning antenna theory, analysis, design and measurements.

Dr. Kildal was awarded Best Paper Awards by the IEEE (1985 R.W.P. King Award and 1991 Schelkunoff Prize Paper Award). In 2011 he was awarded the prestigious Distinguished Achievements Award from the IEEE Antennas and Propagation Society. He organizes and lectures in courses within the European School of Antenna (ESoA, www.antennasvce.org).
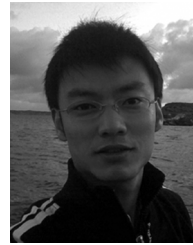
Xiaoming Chen received the B.Sc. degree from Northwestern Polytechnical University, Xi'an, China, and the M.Sc. and Licentiate of Engineering degrees from Chalmers University of Technology, Gothenburg, Sweden, in 2006, 2007, and 2010, respectively.

He joined the Antenna group, Chalmers University of Technology, as a Ph.D. candidate in January 2008. He has authored/coauthored more than 20 journal and conference papers. His research areas include reverberation chamber for OTA measurements, and multi-antenna channel characterizations.

Charlie Orlenius (M'10) was born in Vrigstad, Sweden, in 1976. He received the Master of Science degree in engineering physics from Chalmers University of Technology, Gothenburg, Sweden, in 2001.

Since 2001, he has been with Bluetest AB, Gothenburg, Sweden, working with research and development of reverberation chambers for testing of small antennas and wireless units. Currently, he holds the position of Chief Technology Officer at Bluetest. He is also with the Antenna Group, Department of Signals and Systems, Chalmers University of Technology, participating in the research activities regarding reverberation chambers. He is the author and coauthor of a large number of papers, book chapters and conference contributions about measurements in reverberation chamber.

Magnus Franzén received the M.S. degree in engineering physics from Chalmers University of Technology, Gothenburg, Sweden, in 2005. During his master thesis project he studied and developed tracking antennas at the German company JDA Systems.

In 2005, he was hired by Bluetest AB, Gothenburg, Sweden, to work with the development of over the air tests in reverberation chambers. He is currently the Manufacturing Director of Bluetest and also works as a reverberation chamber expert in standardization organizations, such as CTIA and 3GPP.

Per-Simon Kildal (M'76–SM'81–F'95) received the M.S.E.E., Ph.D., and Doctor Technicae degrees from the Norwegian Institute of Technology, Trondheim, Norway, in 1976, 1982, and 1990, respectively.

Since 1989, he has been a Professor of antennas at Chalmers University of Technology, Gothenburg, Sweden, where he is the current Head of the Antennas Group. His main tasks are to lead and supervise research and education within antenna systems. Until now, 18 graduate students have received a Ph.D. from him. He has done the electrical design of the 40 m × 120 m cylindrical reflector antenna and line feed of the EISCAT scientific organization, and the dual-reflector Gregorian feed of the 300 m Ø radio telescope in Arecibo. He is the inventor behind technologies such as dipole with beam forming ring, the hat antenna, and the eleven feed. He was the first to introduce the reverberation chamber as an accurate measurement instrument tool for over-the-air characterization of small antennas and wireless terminals for use in multipath environments with fading. He is also the originator of the concept of soft and hard

Christian S. Lötbäck Patané received B.S. and M.S. degrees in engineering physics from Chalmers University of Technology, Gothenburg, Sweden, in 2008 and 2010, respectively. For his masters thesis work, he studied reverberation chamber measurement uncertainties and parameter estimations at the National Institute of Standards and Technology in Boulder, CO.

In 2010, he began working at Bluetest AB, Gothenburg, Sweden, which develops and manufactures reverberation chambers for commercial use. Currently, he is working as an R&D engineer, developing hardware and measurement procedures for the reverberation chamber. He is also participating in standard organizations, such as CTIA and 3GPP, as a reverberation chamber expert.